JOURNAL OF Applied Polymer SCIENCE

Catalytic Oxidation of Thioanisole Using Oxovanadium(IV)-Functionalized Electrospun Polybenzimidazole Nanofibers

Ryan S. Walmsley,[1] Percy Hlangothi,[2] Christian Litwinski,[1] Tebello Nyokong,[1] Nelson Torto,[1] Zenixole R. Tshentu[1]

[1]Department of Chemistry, Rhodes University, Grahamstown, 6140, South Africa

[2]Department of Chemistry, Nelson Mandela Metropolitan University, Port Elizabeth, 6031, South Africa

Correspondence to: Z. R. Tshentu (E-mail: z.tshentu@ru.ac.za) (or) R. S. Walmsley (E-mail: ryan.walmsley2@sasol.com)

ABSTRACT: Polybenzimidazole fibers, with an average diameter of 262 nm, were produced by the process of electrospinning. These fibers were used as a solid support material for the immobilization of oxovanadium(IV) which was achieved via a reaction with vanadyl sulfate. The oxovanadium(IV)-functionalized nanofibers were used as heterogeneous catalysts for the oxidation of thioanisole under both batch and pseudo-continuous flow conditions with great success. Under batch conditions near quantitative oxidation of thioanisole was achieved in under 90 min, even after four successive catalytic reactions. Under continuous conditions, excellent conversion of thioanisole was maintained throughout the period studied at flow rates of up to 2 mLh^{-1}. This study, therefore, proposes that electrospun polybenzimidazole nanofibers, with their small diameters, impressive chemical and thermal stability, as well as coordinating benzimidazole group, may be a desirable support material for immobilization of homogeneous catalysts. © 2012 Wiley Periodicals, Inc. J. Appl. Polym. Sci. 000: 000–000, 2012

KEYWORDS: electrospinning; nanofibers; oxovanadium; polybenzimidazole; catalysis

Received 14 March 2012; accepted 18 May 2012; published online
DOI: 10.1002/app.38067

INTRODUCTION

The Merrifield-based microspherical resins were developed for use primarily in solid phase synthesis; however, this work simultaneously stimulated the development of polymer-supported metal-based catalysts.[1,2] Typically, a ligand containing a reactive side group is attached to the polymer support by an alkylation reaction and subsequently reacted with a metal salt to afford the metal-immobilized catalyst.[2–4] While these microspherical beads have been hugely successful when applied to several different reactions,[3,5–7] there remains a need for miniaturizing the catalyst supports thereby improving the surface area-to-volume ratio and hence improving the number of exposed catalytic sites.[8] This has been achieved in part by reducing the diameter of the polymer beads into the nanometer domain; however these resins can be tedious to recover due to their small size.[9]

Recently there has been a renewed interest in electrospinning as a technique for producing polymer nanofibers. These fibers are nano only in diameter and form a mat like three-dimensional structure making separation from solution very simple[10] and as such ideal candidates as catalyst supports.

Several researchers have utilized electrospun fibers for catalytic purposes,[11–16] however most of these are based on metal-oxide or nanoparticle-embedded fibers.[11–15] In contrast, there are few examples in which a coordination based metal-immobilization strategy, similar to that of the before mentioned Merrifield approach, has been adopted. Raston and coworkers[16] made use of this approach, exploiting the free amine and hydroxyl groups of chitosan nanofibers to complex Pd(II). These materials successfully catalyzed a Heck cross-coupling reaction between iodobenzene with *n*-butyl acrylate. In addition to this, we have recently prepared poly(styrene-*co*-vinylimidazole) fibers which were used to immobilize oxovanadium(IV).[17] These fibers successfully catalyzed the oxidation of thioanisole but displayed relatively low mechanical stability and were soluble in multiple solvents. Both of these factors limit the practical use of these materials as catalysts. The drive was therefore to make use of a more resilient polymer that still contained the necessary imidazole functional groups for metal immobilization.

Polybenzimidazole (PBI) (Figure 1) was commercially developed by Celanese Corporation in 1983. It is a heterocyclic polymer with excellent chemical and thermal stability and has been used

Additional Supporting Information may be found in the online version of this article.

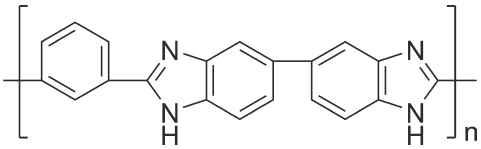

Figure 1. The chemical structure of *m*-polybenzimidazole (PBI).

as a fire-retardant material and more recently in fuel cell membranes.[18] These properties, along with the coordinating ability of the benzimidazole group, make this polymer an excellent candidate as a metal catalyst support. Sherrington's group[19–21] as well as many others,[22–24] have exploited the microspherical forms of this polymer as a support for a range of different metal-catalyzed reactions with great success. Nanofibers of polybenzimidazole[25] and polybenzimidazole/silica[26] composites have been produced by electrospinning but as of yet, have not been applied as catalyst supports.

We have prepared polybenzimidazole nanofibers by electrospinning. These were subsequently reacted with vanadyl sulfate to afford the oxovanadium(IV)-immobilized fiber mat which was thoroughly characterized using scanning electron microscopy (SEM), infrared spectroscopy (IR), thermal gravimetric analysis (TGA) and X-ray photoelectron spectroscopy (XPS) among other techniques. The catalytic activity of the fibrous mats was evaluated for the hydrogen peroxide facilitated oxidation of thioanisole under batch and continuous flow conditions.

EXPERIMENTAL

Materials

Polybenzimidazole (PBI) was purchased from PBI Performance Products (Charlotte, NC) with intrinsic viscosity of 0.8 dL g^{-1}. *N, N*-Dimethylacetamide (DMAc) was purchased from Merck. All other chemicals and solvents were purchased from commercial sources (either Merck Chemicals or Sigma-Aldrich) and used without further purification. Aqueous 30% hydrogen peroxide was standardized by titration with potassium permanganate and found to have an actual concentration of 29.5%.[27]

Instrumentation

The infrared spectra were recorded on a Perkin Elmer 100 ATR-FTIR. The vanadium content was determined using a Thermo Electron (iCAP 6000 Series) inductively coupled plasma (ICP) spectrometer equipped with OES detector. Wavelengths with minimum interferences were chosen (290.88 nm, 292.40 nm, 309.31 nm, 311.07 nm) and three repeats were performed at each wavelength. Progress of the catalyzed reactions was monitored using an Agilent 7890A gas chromatograph (GC), fitted with a flame ionization detector (FID) and a Zebron, ZB-5MSi, capillary column (30 m × 0.25 mm × 0.25 μm). Microanalysis was carried out using a Vario Elementar Microcube ELIII. The electrospun nanofibers were imaged using a TESCAN Vega TS 5136LM scanning electron microscope (SEM). X-ray photoelectron spectra (XPS) were recorded on a Kratos Axis Ultra using an Al Kα radiation with pass energy of 160 eV. Nitrogen adsorption/desorption isotherms were measured at 77 K using a Micromeritics ASAP 2020 Surface Area and Porosity Analyzer. Prior to each measurement, samples were degassed at 150°C for 1 week. The surface area (BET), total pore volume and pore size distribution were calculated from these isotherms. Thermal analysis was conducted using a TA Instruments SDT Q600 at a heating rate of 10°C min^{-1} using nitrogen as a purge gas.

Electrospinning of Polybenzimidazole Nanofibers

PBI (2.0 g) and lithium chloride (0.4 g, 4% wt/vol) were refluxed in DMAc (10 mL) for a period of 5 h. The solution was allowed to cool slightly and then centrifuged to separate undissolved polymer. The viscous polymer solution was then poured into a 20-mL syringe and electrospun at the following conditions. A voltage of 15 kV was applied to the needle tip which had an internal diameter of 0.5 mm. A negative voltage of −5 kV was applied below a rotating drum collector covered with aluminum foil (Figure 2). The distance between the needle and collector was 12 cm. The nanofiber membrane was peeled off the aluminum foil, sandwiched between two pieces of filter paper (to keep the mat flattened) and immersed in methanol overnight to remove residual solvent and lithium chloride and finally dried in an oven at 60°C overnight. The fibers were a brownish-yellow color. *Anal.* Found: C 68.06%, H 5.11%, N 15.17%. IR (ν, cm^{-1}): 1629, 1538, 1444 (C=N, C=C).

Functionalization of PBI_f Nanofibers with Oxovanadium(IV) (PBI_f-VO)

The PBI_f fibers (0.5 g) were added to a solution containing $VOSO_4$ (0.54 g, 2.5 mmol) in methanol (40 mL) and heated to reflux for 24 h under an argon atmosphere. The vanadium functionalized fibers were rinsed with hot methanol several times to ensure complete removal of unreacted vanadium salt. The fibers were then dried in an oven for 48 h at 60°C. *Anal.* Found: C 43.32%, H 4.91%, N 9.32%, S 7.51%. IR (ν, cm^{-1}): 1634, 1566, 1457 (C=N, C=C); 1103, 1036 (SO_4), 978 (V=O).

Catalysis Experiments

Batch Reactions. These reactions were carried out in a similar method as before.[28] In a typical batch reaction, 20 mL of acetonitrile was added to a 50 mL round bottom flask. The temperature of the vessel was maintained at 25°C using a hotplate-stirrer fitted with an external temperature probe. Thioanisole

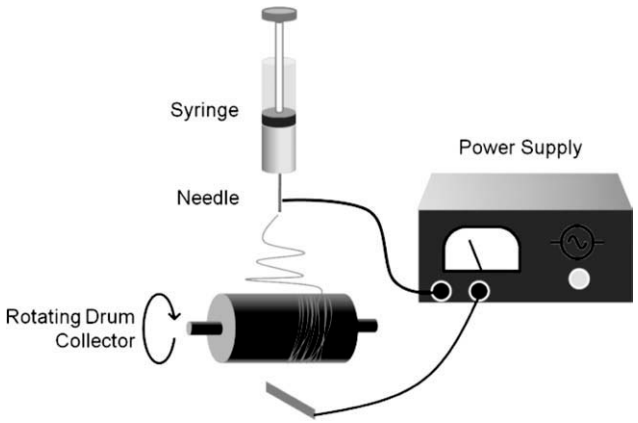

Figure 2. Electrospinning apparatus used in this study. The positive voltage was applied to a needle (0.5 mm internal diameter) and the fibers were collected on a rotating drum collector. A negative potential was applied below the collector to direct the fibers.

Figure 3. The continuous flow set-up used in this study. PBI_f-VO fibers were packed into a filter holder (upper left) and a reactant solution consisting of thioanisole and H_2O_2 in CH_3CN was passed through this. See Supporting Information material for color image.

(0.124 g, 1 mmol) was added followed immediately by PBI_f-VO and 30% H_2O_2 (2 mmol). The stirring rate was kept constant at 100 rpm throughout the reaction. Aliquots were withdrawn at regular time intervals and analyzed by GC.

Continuous Flow Reactions. The PBI_f-VO fibers were packed into a filter holder (Millipore Swinnex® 13) and firmly compressed. In a separate vial, thioanisole (0.124 g, 1 mmol) and 30% (wt) aqueous H_2O_2 (2 mmol) were mixed in acetonitrile for 5 min. This reactant solution was transferred to a 20-mL syringe and the filter holder containing the fibers was connected as shown in Figure 3. The reactant solution was passed through the catalyst bed at a controlled rate by use of a syringe pump (New Era NE-1000). The product solution was collected in individual 0.5 mL fractions and each was analyzed by GC. The temperature of the room was maintained at 25°C throughout the course of the reaction.

RESULTS AND DISCUSSION

Electrospinning and Characterization

Polybenzimidazole is perfectly suited for use as a catalyst support. This polymer displays excellent thermal, physical, and chemical stability[29] and also contains the necessary functional groups to bind the catalytically active metal. The latter characteristic has been exploited in the past;[19,20] however, until now, only the microspherical form of polybenzimidazole has been used as a catalyst support material.

A polybenzimidazole (PBI) solution was prepared by refluxing PBI and LiCl in DMAc for 5 h under argon. After allowing to cool, the mixture was centrifuged and then carefully decanted into a syringe, leaving the undissolved PBI pellet behind thus making the final concentration slightly less than 20 wt % (wt/vol). Several electrospinning parameters were adjusted until a stable jet was achieved. These parameters included; applied voltage, tip-to-collector distance, flow rate and the type of collector used. When a static metal plate collector was used, the fibers did not collect evenly over the surface of the plate but rather began to "climb" towards the spinneret. Since the flow rate was very low, this may have been due to overvoltage.[26] This was circumvented by using a rotating drum collector which concomitantly allowed for partial alignment of the fibers. At low applied voltages (<15 kV), droplets rather than fibers formed, possibly due to insufficient charges present and hence an inability to overcome the surface tension of the solvent. Similarly, at high flow rates, a combination of both fibers and droplets formed. While other research groups have found distances of 6–7 cm to be effective for electrospinning PBI,[25,26] we found 12 cm to give the most stable jet. Given that DMAc is a high boiling point solvent, this extra distance may also improve solvent evaporation. Although not controlled in this study, the ambient conditions, most notably humidity, affected the stability of the polymer jet. The most favorable conditions were obtained when using an applied voltage of 15 kV (and −5 kV underneath the rotating drum), a tip-to-collector distance of 12 cm and a flow rate of 0.15 m L h^{-1}. Following electrospinning, the sheet of fibers was peeled off the aluminum foil, sandwiched between two pieces of filter paper (to keep the mat flat) and soaked in methanol overnight to remove residual solvent and LiCl. The fiber mat was smooth and brown in color (Figure 4) with a very different texture to the polystyrene-based fibers.[17]

The morphology of PBI_f electrospun nanofibers was investigated by scanning electron microscopy (SEM) (Figure 4). The average fiber diameter was found to be 262 nm ($n = 25$), with a relatively broad range of 120–430 nm. A histogram illustrating the fiber diameter distribution can be found in the Supporting Information material section (Supporting Information Figure S1). Similar results were reported by both Weber[26] and Reneker.[25] The specific surface area (BET) for the PBI_f and PBI_f-VO was 7.5 and 7.7 m^2 g^{-1}, respectively. The pore volume and size were 0.041 cm^3 g^{-1} and 232 Å for PBI_f and 0.052 cm^3 g^{-1} and 228 Å for PBI_f-VO (Supporting Information Figures S2 and S3).

Infrared analysis of PBI_f clearly confirmed the presence of the imidazole N—H stretch at 3400 cm^{-1} as well as the expected benzimidazole ring stretching vibrations between 1635 and 1500

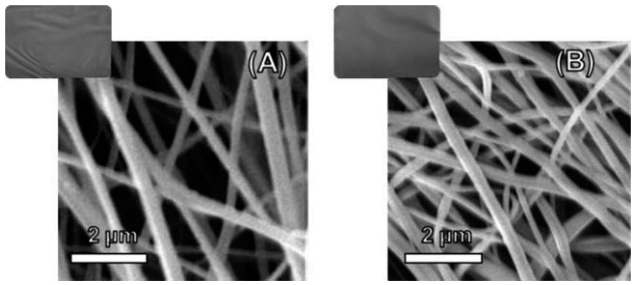

Figure 4. SEM images of (A) PBI_f and (B) PBI_f-VO. Inserts show digital images of the corresponding fibrous membranes. See Supporting Information for color image.

Applied Polymer SCIENCE

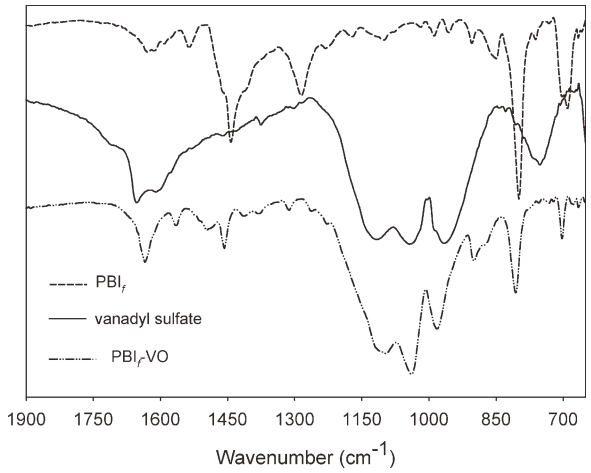

Figure 5. Infrared spectra of PBI$_f$, vanadyl sulfate and PBI$_f$-VO.

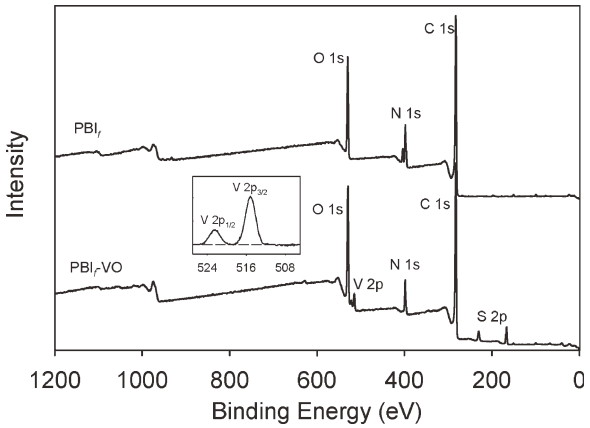

Figure 6. XPS wide scan spectra of PBI$_f$ (top) and PBI$_f$-VO (bottom). Insert shows high resolution scan of the V 2 p signal of PBI$_f$-VO.

cm^{-1}.[29,30] An O—H stretch at 3619 cm^{-1} was due to absorbed water owing to the hygroscopic nature of PBI. After reacting PBI$_f$ with vanadyl sulfate, several new bands appeared including the ν(V=O) at 978 cm^{-1} along with an intense split band at 1103 and 1036 cm^{-1} corresponding to the coordinated sulfate stretching vibrations (Figure 5).[31]

Microanalysis also confirmed the presence of sulfur in the polymer while the vanadium content, which was determined using ICP-OES, was found to be 5.5%, corresponding to a *V/N* ratio of 1:6. Wide scan and high resolution XPS spectra of PBI$_f$ and PBI$_f$-VO are shown in Figures 6 and 7, and confirm surface modification of the fibers. For PBI$_f$-VO the peaks corresponding to the S 2 p, V 2p$_{3/2}$, and V 2p$_{1/2}$ binding energies appeared at 166, 515.2, and 522.6 eV, respectively (Figure 7). The V 2p$_{3/2}$ binding energy further supported the predicted +4 oxidation state of vanadium.[32] There were three resolvable N 1 s peaks for PBI$_f$ appearing at 405, 399, and 396 eV (Figure 7). The more intense peak at 399 eV possibly corresponded to the N—H (amine) nitrogen while the remaining two peaks (at 405 and 396) possibly corresponded to the C=N (imine) nitrogen (possibly protonated and deprotonated). Upon coordination, however, the peak at 405 eV disappeared completely while the peak at 396 eV was significantly diminished, confirming coordination of vanadyl via the azomethine nitrogen.

Thermogravimetric analysis of PBI$_f$ and PBI$_f$-VO was conducted under a nitrogen atmosphere in a temperature range of 30–800°C (Figure 8). For PBI$_f$, three distinct weight losses were observed at below 105°C, between 220 and 320°C and finally between 570 and 800°C. The first two weight loss can be assigned to loss of loosely bound or coordinated water molecules, since it is well known that PBI readily absorbs moisture even after extensive drying.[33,34] As has been reported by others,[34,35] it was only at temperatures of greater than 570°C that the polymer backbone began to degrade demonstrating the significant thermal stability of PBI. For PBI$_f$-VO there were once again three distinct weight loss processes occurring (Figure 8). As was the case for the unmetallated PBI$_f$ fibers, the first weight loss occurred below 105°C due to loss of water. The weight loss occurring between 270–490°C, was however unique to the oxovanadium(IV) functionalized PBI$_f$-VO fibers and may be due to decomposition of the bound vanadium salt.[36,37]

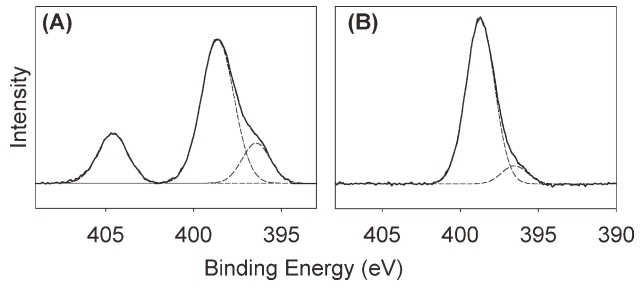

Figure 7. High resolution XPS spectra of (A) N1s signal of PBI$_f$ and (B) N1s signal of PBI$_f$-VO.

Catalytic Activity

The oxidation of sulfides is a useful reaction both for the preparation of biologically active precursors,[37] as well as for sulfur removal from fuels by oxidative desulfurization.[38–40] The latter has become extremely important with current environmental concerns and more stringent regulations. The model reaction used to test the efficacy of the catalyst for sulfide oxidation was the hydrogen peroxide facilitated oxidation of thioanisole. Thioanisole can be converted to methyl phenyl sulfoxide, which may subsequently be oxidized to methyl phenyl sulfone. Significant research has been conducted using vanadium as a catalyst for this reaction,[28,41] with the catalytic mechanism having been thoroughly studied.[38,42]

Stirred-Batch Reactions. The catalytic activity of the PBI$_f$-VO nanofibers was first investigated using a typical stirred-batch reaction similar to our previous work.[28,41] The mass of the catalytically active fibers was varied from 0.010 g to 0.050 g. This equates to approximately 1.0–5.3 mol % of vanadium relative to thioanisole, respectively. At all catalyst masses, near quantitative conversions were obtained with turnover frequencies (TOF's) of 88.39, 36.70, and 36.71 h^{-1} for 0.010 g, 0.025 g, and 0.050 g respectively. At the higher mass (0.050 g); however, the reaction was near complete in just 30 min compared with 1 h at the

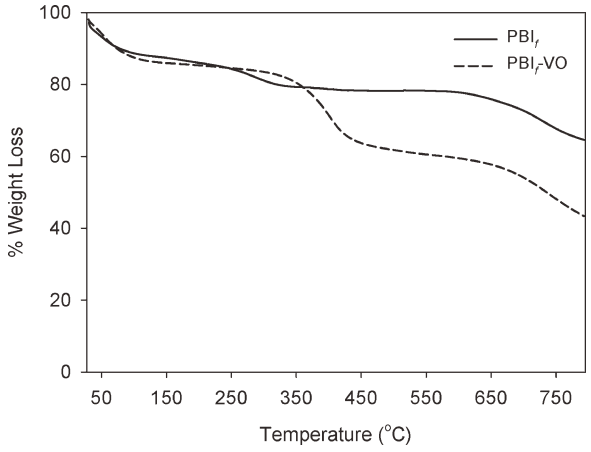

Figure 8. TGA curves for (A) PBI$_f$ and (B) PBI$_f$-VO.

lower catalyst masses (0.010 and 0.025 g) (Figure 9). When the oxovanadium functionalized nanofibers were substituted with the unfunctionalized PBI nanofibers (PBI$_f$), a maximum conversion of 9.12% was observed after 90 min, illustrating the catalytic effect of vanadium. The recyclability of the fibers was also investigated as shown in Figure 10. An initial drop in activity was observed after the first cycle following which the conversion remained fairly constant; this was likely related to the initial leaching, which will be addressed later. Despite the much improved mechanical stability of the PBI fibers compared to polystyrene-based fibers, after a few successive runs there was some catalyst deterioration. The fine paper-like texture of the nanofiber mat was undeniably more suited to a continuous flow system rather than being subjected to mechanical agitation.

Continuous Flow Reactions. Since the larger mass of fibers (0.050 g) gave faster initial conversion under batch conditions (Figure 9), this mass was used for the continuous flow reactions. As shown in Figure 11, excellent conversion of thioanisole was obtained over the tested period. At flow rates of between 0.5–2 m L h^{-1}, greater than 98% oxidation of thioanisole was

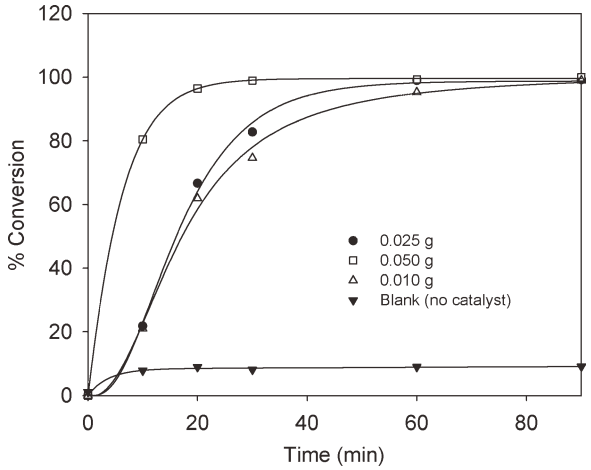

Figure 9. Effect of the amount of PBI$_f$-VO used in the batch reactions. Conditions: thioanisole (1 mmol), H_2O_2 (2 mmol), acetonitrile (20 mL), and 25°C.

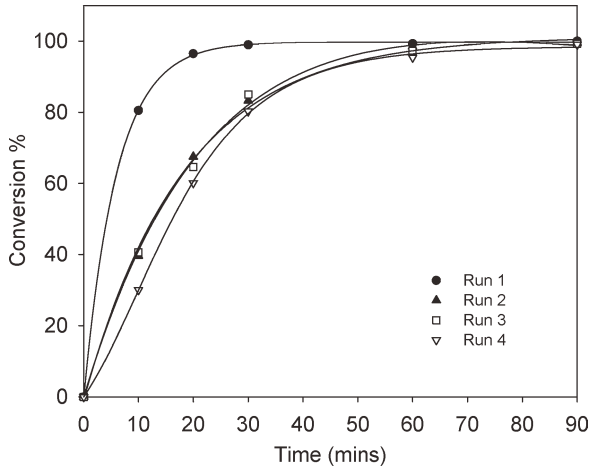

Figure 10. Oxidation of thioanisole under batch conditions showing the catalyst recyclability after successive reactions. Conditions: PBI$_f$-VO (0.05 g), thioanisole (1 mmol), H_2O_2 (2 mmol), CH_3CN (20 mL), and 25°C.

achieved. Furthermore, the product selectivity could be partially tuned by adjusting the flow rate. At a flow rate of 0.5 m L h^{-1}, for example, the ratio of sulfoxide/sulfone was 0.41, while at a higher flow rate of 4 m L h^{-1} this ratio shifted to 2.13, along with a slight drop in overall oxidation (Table I). For comparative purposes, aliquots were withdrawn from the syringe before the reactant solution had passed through the catalyst bed, representing the uncatalyzed reaction. In the 5th,10th, and 20th fraction, a total oxidation of 9.0%, 9.3%, and 9.4% respectively, was observed. This clearly demonstrated the success of the catalyst.

Leaching Studies. Leaching of the active metal from the solid support is an obvious disadvantage.[43] Not only does this reduce the life span (recyclability) of the material, but it would also introduce metal contaminants into the product solution. Leaching in the context of this study, would likely be due to bond

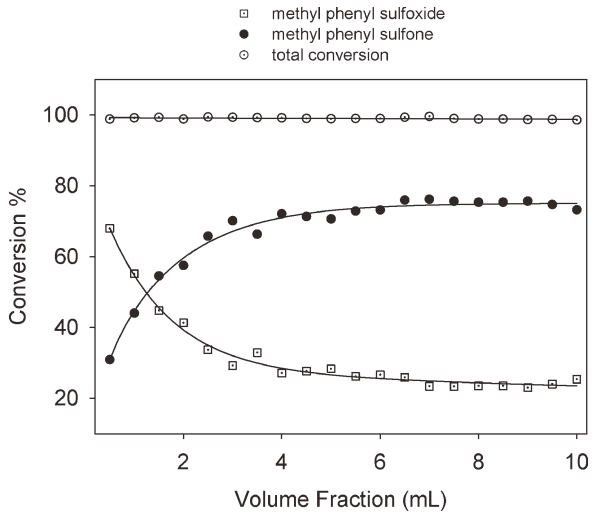

Figure 11. Oxidation of thioanisole under continuous flow conditions including product selectivities. Conditions: PBI$_f$-VO (0.05 g), thioanisole (50 m*M*), H_2O_2 (100 m*M*) in CH_3CN, flow rate (v) = 1 mLh^{-1} and 25°C.

Table I. Summary of Reaction Conversions and Product Selectivities for PBI_f-VO Catalyzed Reactions under Batch and Continuous Flow Conditions

Amount (mg)	Sulfoxide (%)	Sulfone (%)	Max. Conversion (%)[a]	TOF (h^{-1})*
Batch Process				
50	67.23	32.72	99.95	36.7
50[b]	68.03	31.44	99.47	18.3
50[c]	70.36	28.90	99.27	18.1
50[d]	70.39	28.51	98.90	17.7
25	68.23	30.95	99.18	36.7
10	50.99	47.99	98.99	88.4
Amount (mg)	v (mL h^{-1})	Sulfoxide (%)	Sulfone (%)	Avg. Conversion (%)
Continuous flow process				
50	0.5	28.88	69.79	98.68
50	1.0	31.62	67.54	99.00
50	2.0	40.65	58.64	99.20
50	4.0	63.29	29.78	92.83

[a]After 90-min reaction time, [b]After one successive catalytic reactions, [c]Two successive catalytic reactions. [d]Three successive catalytic reactions, *The TOF was determined as moles of substrate converted/moles of vanadium (determined by ICP-OES) in catalyst/time (h).

attack by hydrogen peroxide along with acidification of the reaction media.[43] To determine the quantity of vanadium leached, the product fractions were combined, concentrated and digested in nitric acid. After appropriate dilutions, the vanadium content was determined by ICP-OES. Under batch conditions, there was an initial leaching of 7.29% vanadium after the first reaction, followed by leaching of between 0.52 and 0.69% in the subsequent cycles, a similar trend observed by others.[44] Furthermore, this corresponds well to the drop in activity observed during the recycling experiments (Figure 10).

Leaching under continuous flow conditions was also monitored. Here, each of the individual 0.5 mL fractions were combined, concentrated and diluted appropriately. Between 0.376%–0.808% vanadium leaching was recorded depending on the reaction conditions, with more leaching being observed at higher flow rates. This small degree of leaching would contribute only slightly to the overall oxidation conversions observed. Additionally, the degree of leaching under continuous flow conditions was markedly less than under batch conditions.

CONCLUSIONS

We have successfully prepared oxovanadium-immobilized polybenzimidazole nanofibers by an electrospinning process. Polybenzimidazole proved to be an excellent support material since it was insoluble and resistant to the reaction solvent and chemicals, but soluble in the electrospinning solvent. While not exploited in this instance, these fibers may also be used up to very high temperatures due to their excellent thermal stability. Furthermore, the imidazole functionality proved to effectively anchor the metal as evidenced by very low metal leaching values. The vanadium functionalized nanofibers effectively catalyzed the hydrogen peroxide facilitated oxidation of thioanisole. While the conversion of thioanisole obtained under batch conditions was high, the mechanical agitation inevitably resulted in catalyst degradation. This coupled with the comparatively higher leaching values under batch conditions, renders the continuous flow method the most suitable for this catalyzed reaction.

ACKNOWLEDGMENTS

The authors acknowledge the Department of Science and Technology (DST)/Mintek-National Innovation Centre (NIC) (Rhodes University) for microanalysis, BET and XPS data. The authors are grateful to the Electron Microscopy Unit (Rhodes University) for use of the SEM. The work would not be possible without financial support provided by Sasol and NRF (South Africa).

REFERENCES

1. Sherrington, D. C. *Pure. Appl. Chem.* **1987,** *60*, 401.
2. Maurya, M. R.; Kumar, A.; Costa Pessoa, J. *Coord. Chem. Rev.* **2011,** *255*, 2315.
3. Maurya, M. R.; Sikarwar, S.; Kumar, M. *Catal. Comm.* **2007,** *8*, 2017.
4. Maurya, M. R.; Kumar, M.; Arya, A. *Catal. Comm.* **2008,** *10*, 187.
5. Maurya, M. R.; Kumar, U.; Manikandan, P. *Dalton. Trans.* **2006, 3561.**
6. Maurya, M. R.; Arya, A.; Adao, P.; Pessoa, J. C. *Appl. Catal., A* **2008,** *351*, 239.
7. Maurya, M. R.; Arya, A.; Kumar, A.; Pessoa, J. C. *Dalton Trans.* **2009, 2185.**
8. Ebert, K.; Bengtson, G.; Just, R.; Oehring, M.; Fritsch, D. *Appl. Catal., A* **2008,** *346*, 72.
9. Wang, Y.; Chen, J.; Xiang, J.; Li, H.; Shen, Y.; Gao, X.; Liang, Y. *React. Funct. Polym.* **2009,** *69*, 393.

10. Reneker, D. H.; Yarin, A. L. *Polymer* **2008,** *49*, 2387.
11. Formo, E.; Lee, E.; Campbell, D.; Xia, Y. *Nano. Lett.* **2008,** *8*, 668.
12. Formo, E.; Peng, Z.; Lee, E.; Lu, X.; Yang, H.; Xia, Y. J. *Phys. Chem. C* **2008,** *112*, 9970.
13. Formo, E.; Yavuz, M. S.; Lee, E. P.; Lane, L.; Xia, Y. J. *Mater. Chem.* **2009,** *19*, 3878.
14. Obuya, E. A.; Harrigan, W.; Andala, D. M.; Lippens, J.; Keane, T. C.; Jones, W. E., Jr. *J. Mol. Catal. A: Chem.* **2011,** *340*, 89.
15. Fang, X.; Ma, H.; Xiao, S.; Shen, M.; Guo, R.; Cao, X.; Shi, X. J. *Mater. Chem.* **2011,** *21*, 4493.
16. Bradshaw, M.; Zou, J.; Byrne, L.; Swaminathan Iyer, K.; Stewart, S. G.; Raston, C. L. *Chem. Comm.* **2011,** *47*, 12292.
17. Walmsley, R. S.; Ogunlaja, A. S.; Coombes, M. J.; Chidawanyika, W.; Litwinski, C.; Torto, N.; Nyokong, T.; Tshentu, Z. R. *J. Mater. Chem.* **2012,** *22*, 5792.
18. Kim, S.-K.; Kim, T.-H.; Jung, J.-W.; Lee, J.-C. *Polymer* **2009,** *50*, 3495.
19. Miller, M. M.; Sherrington, D. C. *J. Chem. Soc., Chem. Commun.* **1994,** 55.
20. Miller, M. M.; Sherrington, D. C. *J. Catal.* **1995,** *152*, 368.
21. Mbeleck, R.; Ambroziak, K.; Saha, B.; Sherrington, D. C. *React. Funct. Polym.* **2007,** *67*, 1448.
22. Li, N. H.; Fréchet, J. M. J. *J. Chem. Soc., Chem. Commun.* **1985,** 1100.
23. Magdalene, R. M.; Leelamani, E. G.; Nanje Gowda, N. M. *J. Mol. Catal. A: Chem.* **2004,** *223*, 17.
24. D'Archivio, A. A.; Galantini, L.; Biffis, A.; Jeřábek, K.; Corain, B. *Chem. Eur. J.* **2000,** *6*, 794.
25. Kim, J.-S.; Reneker, D. H. *Polym. Eng. Sci.* **1999,** *39*, 849.
26. von Graberg, T.; Thomas, A.; Greiner, A.; Antonietti, M.; Weber, J. *Macromol. Mater. Eng.* **2008,** *293*, 815.
27. Reichert, J. S.; McNeight, S. A.; Rudel, H. W. *Ind. Eng. Chem.* **1939,** *11*, 194.
28. Tshentu, Z. R.; Togo, C.; Walmsley, R. S. *J. Mol. Catal. A: Chem.* **2010,** *318*, 30.
29. Thomas, C. In High-Performance Fibers; Hearle, J. W. S., Ed.; Woodhead Publishing: Cambridge, **2001;** Chapter 9, p 310.
30. Sannigrahi, A.; Ghosh, S.; Maity, S.; Jana, T. *Polymer* **2010,** *51*, 5929.
31. Nakamoto, Z. Infrared and Raman Spectra of Inorganic and Coordination Compounds; Wiley: New York, **1978.**
32. Groenenboom, C. J.; Sawatzky, G.; de Liefde Meijer, H. J.; Jellinek, F. J. *Organomet. Chem.* **1974,** *76*, C4.
33. Jouanneau, J.; Mercier, R.; Gonon, L.; Gebel, G. *Macromolecules* **2007,** *40*, 983.
34. Sannigrahi, A.; Arunbabu, D.; Sankar, R. M.; Jana, T. J. *Phys. Chem. B* **2007,** *111*, 12124.
35. Lobato, J.; Canizares, P.; Rodrigo, M.; Linares, J.; Aguilar, J. J. *Membr. Sci.* **2007,** *306*, 47.
36. Udupa, M. R. *Thermochim Acta* **1981,** *51*, 169.
37. Srivastava, S.; Pandey, O. P.; Sengupta, S. K. *Trans. Met. Chem.* **1996,** *21*, 262.
38. Kaczorowska, K.; Kolarska, Z.; Mitka, K.; Kowalski, P. *Tetrahedron* **2005,** *61*, 8315.
39. Maurya, M. R.; Arya, A.; Kumar, A.; Kuznetsov, M. L.; Avecilla, F.; Costa, P. J. *Inorg. Chem.* **2011,** *49*, 6586.
40. Pawelec, B.; Navarro, R. M.; Campos-Martin, K. M.; Fierro, J. L. G. *Catal. Sci. Technol.* **2011,** *1*, 23.
41. Walmsley, R. S.; Tshentu, Z. R. S. *Afr. J. Chem.* **2010,** *63*, 95.
42. Maurya, M. R.; Kumar, M.; Kumar, A.; Costa Pessoa, J. *Dalton Trans.* **2008,** 4220.
43. Castro, I. U.; Sherrington, D. C.; Fortuny, A.; Fabregat, A.; Stüber, F.; Font, J.; Bengoa, C. *Catal. Today* **2010,** *157*, 66.
44. Miller, M. M.; Sherrington, D. C. *J. Catal.* **1995,** *152*, 377.